Detection of the Receptor-Binding Domain of the SARS-CoV-2 Spike Glycoprotein at Physiologically Relevant Concentrations Using Surface-Enhanced Raman Spectroscopy

Konstantin Mochalov, Ivan Vaskan, Andrey K Sarychev, Alexandre V Ivanov, Igor V Bykov, Nikolai V Bakholdin, Daria V Vasina, Vladimir A Gushchin, Artem P Tkachuk, Galina Nifontova, et al.

Detection of the Receptor-Binding Domain of the SARS-CoV-2 Spike Glycoprotein at Physiologically Relevant Concentrations Using Surface-Enhanced Raman Spectroscopy

Konstantin Mochalov,[†,¶] Ivan Vaskan,[†,¶] Andrey K. Sarychev,[§] Alexandre V. Ivanov,[§] Igor V. Bykov,[§] Nikolai V. Bakholdin,[‖] Daria V. Vasina,[#] Vladimir A. Gushchin,[#,×] Artem P. Tkachuk,[#] Galina Nifontova, [†,‡] Pavel S. Samokhvalov,[†] Alyona Sukhanova,[‡] and Igor Nabiev [‡,*]

[†] *National Research Nuclear University MEPhI (Moscow Engineering Physics Institute), 115409 Moscow, Russia*

[¶] *Shemyakin–Ovchinnikov Institute of Bioorganic Chemistry, Russian Academy of Sciences, 117997 Moscow, Russia*

[§] *Institute of Theoretical and Applied Electrodynamics, Russian Academy of Sciences, 125412 Moscow, Russia*

[‖] *National Research University "Moscow Power Engineering Institute", 111250 Moscow, Russia*

[#] *Federal State Budget Institution "National Research Centre for Epidemiology and Microbiology named after Honorary Academician N F Gamaleya" of the Ministry of Health of the Russian Federation, 123098 Moscow, Russia*

[×] *Department of Virology, Biological Faculty, Lomonosov Moscow State University, 119234 Moscow, Russia*

[‡] *Laboratoire de Recherche en Nanosciences, LRN-EA4682, Université de Reims Champagne-Ardenne, 51100 Reims, France*

* *e-mail: igor.nabiev@univ-reims.fr*

Surface-enhanced Raman scattering (SERS) spectroscopy is a surface- or cavity-enhanced variant of Raman scattering spectroscopy allowing the detection of analytes with a sensitivity down to single molecules. The main prerequisite for the effectiveness of this method is the development of SERS-active surfaces or cavities capable of concentrating incident radiation into small mode volumes containing the analyte. Here, we have demonstrated that concentration of light in an ultranarrow metal–dielectric nano-cavity between a film of the receptor-binding domain (RBD) of SARS-CoV-2 S

glycoprotein and silver surface, which is formed via interaction of reduced sulfhydryl groups of the RBD with silver, allows recording SERS spectra at concentrations sufficient for ultrasensitive detection of viral protein antigens at physiologically relevant (sub-picogram) levels. Moreover, an additional increase in the cavity Q-factor upon coating the dielectric RBD film with a nanometer-thick silver shell results in an additional order(s) of magnitude enhancement of the protein SERS signal, thus ensuring a sub-femtogram sensitivity of the viral antigen detection. A simplified theoretical model explaining the observed additional enhancement of the SERS signal from the protein coated with a silver film is proposed.

Our study is the first to obtain characteristic Raman and SERS spectra of the RBD of S glycoprotein, the key SARS-CoV-2 viral antigen directly, without the use of low-molecular-weight Raman-reporter molecules. The possibility of direct recording of characteristic spectra of viral protein antigens at the concentration orders of magnitude lower than those required for the detection of the whole virus in biological media makes the development of a high-performance optical method for detecting and conformational analyzing the pathogen variants a realistic task.

INTRODUCTION

Three coronaviruses have crossed the species barrier to cause deadly pneumonia in humans since the turn of the 21st century: severe acute respiratory syndrome coronavirus (SARS-CoV) [1, 2], Middle-East respiratory syndrome coronavirus (MERS-CoV) [3], and SARS-CoV-2 [4, 5]. The SARS-CoV infection emerged in the Guangdong province of China in 2002 and spread to five continents through air travel routes, infecting 8,098 people and causing 774 deaths. In 2012, MERS-CoV caused an epidemic in the Arabian Peninsula, where it still remains a major public health concern, and spread to 27 countries, infecting a total of 2,494 individuals and claiming 858 lives. Finally, a previously unknown coronavirus, named SARS-CoV-2, was discovered in December 2019 in Wuhan, the Hubei province of China. SARSCoV-2 is responsible for the ongoing outbreak of atypical pneumonia (COVID-2019) that has affected over 245 million people and killed about 5 million in more than 220 countries worldwide as of October 18, 2021 (www.worldometers.info/coronavirus/). Recurrent spillovers of coronaviruses in humans, together with findings of numerous coronaviruses, including SARS-like ones (SARSr-CoV) in bats, suggest that future zoonotic transmission events may occur [6].

The global world pandemic situation related to COVID-19 could have been prevented if large-scale, quick diagnosis of active infection cases had been possible. This further confirms that more efficient methods for detecting viral infections are to be developed. The existing immune [7] and molecular [8] assays, including

ELISA [9] and PCR [10], are sufficiently sensitive for the identification of coronaviruses but require prior knowledge of the strains. Deep sequencing techniques [11] are powerful tools of virus surveillance that can detect mutations in virus genomes and capture information on genetic diversity in the virus population if the sequence coverage is sufficient. However, the low virus titer in most samples leads to sequence reads that are dominated by the host genetic material rather than by that of the viral pathogens, and the processing of clinical samples is time-consuming, requires expensive reagents, and involves high technical expertise. The development of a highly sensitive and specific spectral method for quick detection of coronaviruses, particularly SARS-CoV-2 strains, could reduce both the time and the cost of detection, ensure earlier diagnosis, and save many lives.

The selection of the optimal spectral detection object in the virus that would not only allow an intense optical signal to be obtained, but also have spectral differences for viruses of different strains is the key task in developing a highly sensitive and specific quick diagnostic method. Coronavirus entry into host cells is mediated by cell interaction with the spike (S) glycoprotein, which protrudes outside the virus envelope [12] and includes a receptor-binding domain (RBD) ensuring the recognition of the cell receptor, fusion of the virus and cell membranes, and virus entry into the cell (Figure 1). Because the coronavirus S glycoprotein (including its key component, the RBD protein) is exposed on the surface and is involved in virus entry into host cells, it is the main target of neutralizing antibodies during infection and the focus of drug and vaccine development. At the same time, the possible differences in the structural organization or morphology of the SARS-CoV-2 S glycoprotein from the S glycoproteins of other viral strains can be considered as a basis for developing the diagnostics of specific viral strains and variants.

It has been widely recognized that optical sensing technologies may hold the key to the development of rapid, high-throughput, easy-to-use, point-of-care diagnostics. A number of surface-enhanced Raman scattering (SERS) spectra of biological molecules, including amino acids, peptides; water-soluble, membrane, and glycosylated proteins; nucleotides, oligonucleotides, and double-stranded and single-stranded DNAs, as well as SERS spectra of viruses, bacteria, and drug compounds [13–15], have been published since the early 1980s. The demonstrated possibility of recording the SERS spectra of glycoproteins with a sensitivity down to their concentration in single virions [16–18], as well as the recently developed equipment and technologies for molecular analysis of substances based on tip-enhanced Raman spectroscopy (TERS) [19, 20], has made the ambitious task of specific optical detection of the SARS-CoV-2 S glycoprotein within seconds a reality. However, to date, only a handful of studies have reported the detection of SARS-CoV-2 viral particles or its protein antigens at physiologically relevant concentrations. Two optical sensing approaches have been applied to the detection of SARS-CoV-2 antigens, one based on surface plasmon resonance (SPR) and the other based on SERS [see, e.g., 21–27]. The most sensitive

SERS detection of SARS-CoV-2 and its spike and nucleocapsid proteins was achieved using silver–copper microstars over 400 nm in size, i.e., of the order of the virion size [24]. Importantly, all the SERS studies dealing with the detection of SARS-CoV-2 viral particles, or its protein antigens published to date either are indirect using so-called "SERS-tags" and observing the signals not from the proteins but from the low-molecular-weight Raman-reporters [21, 22, 24-27] or fail to demonstrate typical protein spectra [23]. Application of such indirect approaches make the studies of the viral antigen proteins structure and its difference for different viral variants impossible.

For the best of our knowledge, our study is the first to obtain typical and characteristic Raman and SERS spectra of the RBD of S glycoprotein, the key SARS-CoV-2 viral antigen. An approach has been developed that allows the formation of metal–dielectric microcavities via the interaction of reduced thiol groups of the S-glycoprotein RBD with a SERS-active silver surface, which makes it possible to obtain SERS spectra at concentrations sufficiently low for detecting viral protein antigens at physiologically relevant (sub-picogram) levels. Moreover, we have demonstrated the possibility of increasing the metal–dielectric microcavity Q-factor by coating the dielectric RBD film with a nanometer-thick silver shell, which resulted in an additional order(s) of magnitude enhancement of the RBD SERS signal. A simplified theoretical model qualitatively describing the observed additional enhancement of the SERS signal from the protein coated with a thin silver film is proposed. The possibility of direct recording of characteristic spectra of viral protein antigens at the concentrations orders of magnitude lower than those required for the detection of the whole virus in biological media makes the development of a high-performance optical method for detecting and conformational analyzing the pathogen variants a realistic task.

MATERIALS AND METHODS

SARS-CoV-2 RBD. The recombinant RBD is an Arg319–Phe541 fragment of the S1 spike glycoprotein of SARS-CoV-2 fused to a His6 tag at the C-terminus (Figure 1) [28]. The RBD sequence and physico-chemical properties are presented in the supplementary Table S1. The recombinant RBD was expressed in mammalian cells and purified using metal affinity chromatography (RBD lot no. 8COV1, HyTest, Russia). The protein molecular weight was calculated to be 25,921 Da (including the histidine residues); the purity of the protein preparation was more than 95%.

About 1 mg of protein was dissolved in 140 μl of ultrapure water (MilliQ, 18.2 mΩ cm) additionally filtered through 0.22-μm Millipore filters (Merck, Germany) and transferred into 0.01 M phosphate buffer solution (pH 7.2) using gel-filtration chromatography by means of PD MiniTrap G-25 columns (GE Healthcare, UK). The protein concentration in the obtained eluates was determined using the Bradford method by means of a Nanodrop 2000 instrument (Thermo Scientific, USA). Quality control of the protein samples in phosphate buffer solution was

performed by electrophoresis in polyacrylamide gel according to Lammley in the presence of sodium dodecyl sulfate under reducing and nonreducing conditions. Detection was performed using a ChemiDoc XRS+ instrument (Bio-Rad, USA).

Disulfide bonds in the RBD structure, indicated by arrows in Figure 1, were reduced using TCEP (tris(2-carboxyethyl)phosphine hydrochloride) (Thermo Scientific, USA); the sample was purified from excess TCEP and transferred into 0.01 M phosphate buffer solution (pH 6.0) using MiniTrap G-25 columns (GE Healthcare, UK). As a result, a sample of purified RBD protein with reduced disulfide bonds at a concentration of 1.2 mg/ml was obtained.

Preparation and characterization of SERS-active substrates. Cleaned 26×10 mm Menzel Glasser slides (Thermo Scientific, USA) were placed into a vacuum chamber at a pressure of 10^{-2} Torr and were treated by glow discharge at a current of 0.3 A and a power of 1.5 kW for 30 min, after which the pressure was lowered to 2×10^{-5} Torr. Silver was sputtered from a molybdenum crucible for 1.5 min using electron-beam heating at a current of 40 mA and voltage of 8 kV. The thickness of the sputtered silver layer was estimated by the transmission in the optical channel of the test sample at a wavelength of 600 nm to a value of $T \approx 0\%$, which corresponds to a thickness of the silver film of 90–100 nm. After that, the RBD sample was applied onto the silver surface as described below.

If additional silver sputtering over the protein sample was necessary, the slides were placed into a vacuum chamber at a pressure of 2×10^{-5} Torr without glow discharge treatment. Silver was sputtered from a molybdenum crucible for 0.5 min using electron-beam gun heating at a current of 40 mA and voltage of 8 kV. The thickness of the sputtered silver was estimated by the transmission in the optical channel of the test sample at a wavelength of 600 nm to the value of T=50%, which corresponded to the thickness of silver of 10 nm.

After the formation of SERS-active substrates, they were examined by means of optical microscopy and atomic force microscopy (AFM) in order to detect defect-free areas for the application of protein samples. The studies were performed by means of a Probe Optical 3D Correlation Microscopy System, a unique research setup using VIT_P/IR semi-contact "top-visual" AFM probes (TipsNano, Tallinn, Estonia) at a resolution of 512×512 points per scan and a scan rate of 0.8 Hz. As a result, suitable 4×4 mm areas were selected and marked for the positioning procedure before exposure in the protein solution. Figure 2 shows typical AFM images of the metal surface of silver SERS-active substrates. It can be seen that rough metal deposits were formed with lateral sizes of about 0.5 μm and average heights within 10 –30 nm. The silver bumps and pits operate as open plasmon resonators and generate a large local electric field excited by the impinged electromagnetic wave, with the EM field reaching its maxima in metal depressions [29]. These data were subsequently used for identification and analyzing the protein samples applied onto the SERS-active substrates.

Application of the solutions containing the RBD of the SARS-CoV-2 S glycoprotein onto the surface of SERS-active silver-on-glass substrates (Scheme 1). Samples of native RBD contain one free thiol group and four disulfide bonds [20], whereas RBD with reduced four disulfide bonds contains nine free thiol groups. These free thiol groups capable of forming strong S–Ag chemical bonds with silver surfaces (Figure 3) were applied onto the surface of SERS-active substrates by vertical exposure (Scheme 1). The experimental bench for sample application consisted of a substrate mounting system and a system for the lateral positioning and vertical feeding of a drop of protein solution. The substrate was fixed, with the silver SERS-active side down, parallel to the plane of the protein solution drop application. A drop of protein solution (2 μl) was applied onto the hydrophobic cleaned surface of the Parafilm M PM-999 film (Bemis) mounted on a slide (Menzel Glasser, Thermo Scientific). Then, the parafilm with the solution drop on it was positioned in such a way that a defect-free region of the SERS-active silver substrate was strictly above it. The vertical (from bottom upwards) approach of the parafilm carrying the drop of the protein solution resulted in the drop spreading over the parafilm upon touching the SERS-active substrate (Scheme 1). After 5 min of the incubation, the silver SERS substrate was removed from the bench and washed intensely with a stream of MiliQ water for several minutes. The resultant samples were placed into a desiccator equipped with an air evacuation system for 24 h, after which they were used for measurements.

The described approach excludes gravitational deposition of the sample onto the surface of the SERS-active substrate and ensures the formation of a uniform protein molecular layer firmly bound to the substrate surface due to Ag–S chemical bonds. It should be noted that, although the aliphatic index of RBD protein (the relative volume occupied by the aliphatic side chains of its amino acid residues) is 71.2%, the substantial hydrophobic component of this protein (28.8%) [28], which is part of the coronavirus spike interacting with the hydrophobic cell membrane, appears to be sufficient for the formation of the individual protein aggregates on the surface that are seen in AFM images.

Figure 4 shows a typical AFM image of the metal surface of silver SERS-active substrate, where the RBD sample with reduced disulfide bonds was applied to its surface as described above (Scheme 1, Figure 3). The RBD-covered areas contain distinct formations with the standard lateral dimensions of the order of 0.6 μm and a height of about 50 nm, as seen from Figure 4. It is evident that the areas of protein application clearly differ from the original metal surface shown in Figure 2. Furthermore, there is distinct internal structuring of these formations, in which they significantly differ from the inhomogeneities of silver, and which suggests that they are bulk aggregates of RBD protein. Accordingly, the main indication for silver SERS-active areas in an optical image of the studied samples is the presence of well-distinguishable inhomogeneities (about 0.6 μm) against the background within the dirt-free areas of the metal film.

Importantly, the described for reduced RBD vertical (from the bottom to upwards) method for applying samples onto the surface of our SERS-active substrates (Scheme 1, Figure 3) does not work in the case of the native RBD protein where disulfide bonds have not been reduced, and, hence, there are no additional free thiol groups. Such samples of native RBD protein were completely washed off the surface of the SERS-active substrate, and it was impossible to detect any traces of the protein in AFM images of these substrates or SERS signals from them. Therefore, to study the native RBD of the SARS-CoV-2 S glycoprotein, the protein solution was applied in drops (2 μl) directly onto the defect-free areas of SERS-active metal film (Scheme 1), and the film was placed into a desiccator, which was sealed and evacuated immediately after the application of the drops. After incubation in the desiccator for 24 h, the substrates were washed twice for 2 min in water (MiliQ) and placed to the desiccator for another 24 h.

To record conventional Raman spectra of RBD, as a negative control, the protein solution was applied onto the surface of a clean (without metal sputtering) Menzel Glasser slide (Thermo Scientific) and the procedure described above was reproduced.

Mapping the RBD protein samples on the SERS-active substrate surface. Spectral measurements were performed using a WITec 500 Alpha Raman spectrometer based on a confocal microscope with a mapping option; the mapping area was 25 × 25 μm. The combination of a spectrometer with an optical microscope made it possible to focus the laser beam and record the spectra from individual protein globules, or even parts of individual globules. The step between the coordinates in the optical image, as well as in the RS map, was approximately 1 μm. A laser with a wavelength of 785 nm, a power of 2–3 mW, and a 50× objective lens was used for mapping; the signal accumulation time being 2–5 s.

Raman and SERS spectroscopy analysis in a metal–dielectric microcavity. In all experiments, the accumulation time was 1 s and the wavelength of the excitation laser radiation was 785 nm at a power of 5.76 mW. The spectra shown in the figures are the results of averaging over 64 spectra.

RESULTS AND DISCUSSION

The SERS mapping of RBD protein with reduced disulfide bands samples on the surface of the SERS-active substrate (Figure 5) demonstrated a distinct and reproducible Raman signal from individual protein aggregates ~0.6 μm in diameter, with the most intense signals observed at the boundaries of the aggregates. Indeed, the direct contact of the analyte with the plasmonic substrate is important for their short-range interaction and amplification of the Raman signal [15].

The Raman signal from the RBD protein on the metal surface resulted from its interaction with plasmons excited in a depression of the metal film. In other words, the SERS signal of the RBD protein was observed due to the excitation of the plasmon resonance and the enhancement of the electric field in the open resonators formed by depressions in the silver film that were filled with the dielectric RBD protein. Because Raman signals were mainly generated in the regions of RBD that had chemical bonds with the silver depression, the signal had maxima at the boundaries of the globules where the Raman signal was not screened by the RBD globule. The parameters of the deposition of the silver substrate were tuned in such a way as to increase the amplitude of the random plasmon field generated by the impinging light [31], although the substrate should be further optimized.

The sensitivities of Raman and SERS detection of the SARS-CoV-2 RBD

For conventional Raman spectrum recording, the RBD solution was applied dropwise onto a glass slide and dried. As it was mentioned in the Materials and Methods section, although the aliphatic index of RBD (the relative volume occupied by the aliphatic side chains of its amino acid residues) is 71.2%, the substantial hydrophobic component of this protein (28.8%) [28] corresponding to the part of the coronavirus spike interacting with the hydrophobic cell membrane appears to be sufficient for the formation of the protein aggregates with sizes of several hundred micrometers in all dimensions on the silver surface (data not shown). Hence, it can be assumed that the spectra were recorded from a sample volume of ~10^9 nm^3, which corresponded to the excitation volume of the spectrometer. Considering that the volume of the RBD molecule 4 nm in diameter [28] is ~34 nm^3, the conventional Raman spectra of native RBD (Figure 6, spectrum 1) were recorded from (1/34) × 10^9 ≈ **3 × 10^7** molecules, which corresponds to **1.3 pg** of the sample.

The SERS spectra of native RBD (Figure 6, spectrum 2) were obtained from individual protein aggregate. The spectra were recorded from the place of location of the drop of the native protein solution, which was washed out before recording the spectra. The shape of the protein aggregates can be approximately estimated from Figure 4 as segments of spheres with a diameter of 600 nm and a height of

50 nm. The volumes of these aggregates can be estimated as $\mathbf{(1/6) \times \pi \times h \times (3R_2^2 + h^2)}$, where **R2** is the radius of the top circle and **h** is the height of the spherical segment, which gives a volume of less than 2.2 × 10^6 nm^3. Therefore, the signal was recorded from $\mathbf{6.4 \times 10^4}$ molecules of RBD, which corresponded to **2.7 fg** of the sample of RBD protein. In the case of the RBD aggregates with reduced S–S bonds (free SH groups with high affinity for the silver surface), the Raman signal was obtained from the molecules that were in direct contact with the silver surface. This aggregate can be approximately described as a disk 300 nm in radius and 4 nm in height. Using a similar volumetric approach, we can conclude that in this case the quantity of the reduced RBD molecules that could provide the SERS signal can be estimated at about **1 fg** of protein.

In general, the RBD Raman spectrum (Figure 6, spectrum 1) is typical of a water-soluble protein [29]. This spectrum is mainly dominated by the peaks at 1463 cm^{-1} attributed to the C–H stretching and at 1344 cm^{-1} attributed to C–H deformation; it also clearly displays the bands of the tyrosine (at about 858 cm^{-1}), phenylalanine (about 1008 cm^{-1}), amide III (about 1265 cm^{-1}), and amide I (about 1670 cm^{-1}) vibrations. At the same time, no sharp bands at 761, 1330, or 1561 cm^{-1} characteristic of tryptophan residues appear in the Raman spectrum of RBD, which is due to the relatively low tryptophan content of the RBD protein: two tryptophan residues versus 14 phenylalanine residues (see supplementary Table S1 for RBD amino acid composition).

Figure 6 shows comparison of the Raman spectra of the native RBD of SARS-CoV-2 S glycoprotein (spectrum 1) with the SERS spectra of native RBD and RBD with reduced S–S groups, with both samples located on a ~~the same~~ SERS-active metal film (spectra 2 and 3, respectively).As seen from Figure 6, the amplitude of the Stokes lines, measured from the base line, are approximately the same for all three spectra. However, the normalization factor and amount of RBD in each sample differ considerably. Raman spectrum of native RBD (spectrum 1) is obtained from ~1 pg of the protein, whereas the SERS spectrum of native RBD (spectrum 2) is obtained from as little as 1–3 fg of the protein. Therefore, given the close values of the scaling factors of spectra (1) and (2) (126 and 216, respectively), the enhancement factor for the SERS spectrum of native RBD can be estimated as $G_1 \sim 10^3$. Finally, considering that the scaling factor of spectrum (3) is 1, the SERS enhancement factor for RBD with reduced disulfide bonds can be estimated to be at least $G_2 \sim 126 \times G_1 \sim 10^5$, i.e., two orders on magnitude larger than G_1.

In spite of obvious difference between the Raman spectrum of native (spectrum 1) and SERS spectrum of reduced (spectrum 3) RBD, the shape of the SERS spectrum of native RBD is very similar to the shape of the Raman spectrum of this protein (compare the spectra 1 and 2 in Figure 6). In order to

confirm additionally the presence of the SERS spectral effect in the case of native RBD, we analyzed the difference spectrum between the Raman and SERS spectra (spectra (1) and (2) in Figure 6) for native RBD deposited on glass and on the SERS-active surface, respectively (Figure 6, spectrum (4), gray line). One can see that the difference spectrum of the Raman and SERS spectra of native RBD match well in the region of 400–1200 cm^{-1}, yielding a practically flat baseline after subtraction. This region includes characteristic bands of aromatic amino acids Phe, Trp and Tyr and some stretching vibrations of protein backbone. Beyond this region, the difference spectrum shows clear differences between the Raman and SERS signals of the native RBD protein in the regions of C–H stretching, C–H deformation, and amide I vibrations. This confirms the specific interaction of RBD with the SERS-active surface, which should be the origin of the observed enhancement of its Raman signal.

When the RBD protein with four reduced disulfide bonds (see supplementary Table S1) was deposited on the same SERS-active substrate, the shape of its SERS spectrum was completely different from those of both Raman and SERS spectra of the native RBD (Figure 6, spectrum 3). The spectrum is dominated by the previously absent bands of the aromatic amino acid tryptophan (Trp) at about 755, 1340, and 1545 cm^{-1}. The characteristic Phe, Tyr, and amide I signals have completely disappeared, and the amide III vibration at about 1265 cm^{-1} and the C–H deformation vibration at about 1455 cm^{-1} are strongly suppressed. Such a significant change in the Raman spectrum along with its significant enhancement by the surface of the SERS-active substrate, given the absence of enhancement of the native protein signal, indicates the predominant role of directional binding of the reduced RBD to the silver surface through the thiol groups that were formed by reduction of RBD disulfide bonds. A sketch demonstrating this mode of interaction of reduced RBD with the surface of the SERS-active substrate is shown in Figure 3.

As it was noted above, the two orders larger enhancement factor G_2 (SERS of the reduced RBD) in comparison with factor G_1 for the native RBD can be comprehend upon the assumption that the main contribution to G_2 is determined by the direct interaction of RBD fragments with the silver substrate via thiol binding. Therefore, the amount of the RBD protein volume that effectively generates the SERS signal can be assumed to correspond to one molecular monolayer, i.e., 1 fg of RBD. These speculations are further supported by the close similarity between the spectrum (1) of conventional Raman scattering of native RBD and its SERS spectrum (2) (Figure 6). The small difference, explicitly shown in Figure 6 (spectrum (4), gray line), could be attributed to the interaction of the native RBD molecules with the highly inhomogeneous plasmon field excited in the silver SERS substrate [30,31]. On the other hand, the SERS signal of the reduced RBD (spectrum 3 in Figure 6) is not only a hundred times more intense than that of the native RBD, but it has quite a different shape. This could be due to the formation of thiol bonds

between RBD and the SERS substrate, which induce indirect intensity modulation of the Stocks lines from the vibrations that are not physically connected with these bonds. This phenomenon, sometimes called "chemical enhancement", is still widely discussed [32, 33]. However, to our best knowledge, we are the first to observe direct conversion of so-called electromatic long-range enhancement of the protein Raman spectrum to the short-range "chemical" mode of enhancement via specific reduction of protein disulfide bonds what provoked direct interaction of thiol groups with the surface of the SERS-active substrate. Further study of developed approach and discovered phenomenon could shed more light on the nature of this specific SERS effect at enable development of the general approach to switching between two mechanisms of Raman signals enhancement.

A new method for SERS response enhancement upon applying an additional thin metal layer onto the dielectric RBD film on the surface of the SERS-active substrate

Application of an additional, optically transparent (about 10 nm) layer of silver on the protein aggregates formed from reduced RBD moieties containing reactive thiol groups resulted in a substantial further enhancement of the SERS signal. Scheme 1 (right panel) illustrates the procedure of additional silver layer deposition and Figure 5 (bottom panels) demosntrates the procedure of the spectral study of the protein aggregates formed on the SERS-active substrate after additional silver coating. The images obtained in the wide-field upright optical microscopy mode (left bottom panel) and mapping (right bottom panel) based on the characteristic Raman band in the confocal mode are shown. The essence of the procedure consisted in searching for RBD aggregates using a conventional microscope, obtaining a spectrum at the point, mapping the aggregates in the confocal microscopy mode (accumulation time, 0.4 s per point), and then obtaining a spectrum at the point of the highest intensity obtained during the mapping.

The SERS spectrum of a sample of the reduced SARS-CoV-2 RBD with reactive thiol groups upon application of a thin silver film onto the protein sample bound with the SERS-active substrate is shown in Figure 7. It can be seen that the application of the additional silver layer led to an almost tenfold enhancement of the RBD SERS signal compared to the SERS intensity of uncapped RBD. It is noteworthy that the same procedure of deposition of an additional silver layer on the film of native RBD protein located on the same SERS-active substrate resulted in a complete disappearance of the Raman signal.

The effect of additional enhancement of the SERS signal from the reduced RBD coated with an additional silver layer can be explained by an increase in the Q-factor of the metal–dielectric resonator. The Q-factor of metal–dielectric resonators can be increased by decreasing the radiative loss. It is well known that, at optical frequencies, the permittivity of metals is negative. In our case, the conducting

current flows in the silver shell of the resonator, and the polarization current oscillates in the dielectric RBD core. These currents have opposite directions when the metal permittivity is negative. Because the radiation from this resonator is comparable with the sum of the currents, the radiative losses decrease for a resonator when the permittivities of the resonator materials have different signs [34].

We have developed a simple model of SERS in a metal envelope, which is presented briefly below and will be published in full elsewhere. The model qualitatively describes the enhancement of the SERS from the RBD of SARS-Cov-2 spike protein coated with a thin silver film. The theory estimates how the SERS changes when an RBD globule is covered with a metal nanolayer. The radiating molecular dipole interacts with the metal envelope and can excite plasmons in the metal. The plasmon radiation is added to, or subtracted from, the molecular dipole radiation. The plasmon oscillations reach their maximum when the dipole frequency is close to the plasmon resonance of the metal envelope and the dipole itself is close to the plasmon envelope. Then the collective dipole of the electron density oscillations is much larger than the molecular dipole. The overall radiation may be considerably enhanced in this case. This enhancement G_3 is multiplied by the SERS enhancement factor G_2, which is due to the direct interaction of the RBD molecular dipole with the metal surface. That is, the usual SERS signal is multiplied by the factor $G_3 >> 1$.

To estimate the effect of the metal envelope, we use the simplest model, with the radiating dipole placed inside the hollow metal sphere with the radius R and the shell thickness d. The radiation of the dipole is partly reflected back by the sphere and partly goes out. The symmetry of the system allows the electromagnetic field $\mathbf{E}_i$ inside the metal sphere ($r < R$), the field $\mathbf{E}_m$ in the spherical shell ($R < r < R + d$), and the field $\mathbf{E}_e$ outside the sphere ($r > R + d$) to be expanded to Legendre polynomials $P_n(\cos\theta)$. To simplify our model, we neglect the retardation effects inside the sphere and in the metal. In other words, we use the quasi-static approximation for the calculation of the $\mathbf{E}_i$ and $\mathbf{E}_m$ fields for the radius values $r < R + d$. However, the exact solution of the Maxwell equations is used to find the outer fields $\mathbf{E}_e$ and $\mathbf{H}_e$, which extend up to infinity. The electric fields $\mathbf{E}_i$, $\mathbf{E}_m$, and $\mathbf{E}_e$ are found from the boundary conditions at the internal ($r = R$) and external ($r = R + d$) surfaces of the hollow metal sphere. We matched the tangential components of the electric fields and normal components of the electric displacement at the sphere boundaries, obtaining the following dispersion equation determining the n-th resonance:

$$\left(1+\frac{d}{R}\right)^{2n+3} = \frac{(1+n)(2+n)(\varepsilon_1-\varepsilon_m)(\varepsilon_m-\varepsilon_2)}{((2+n)\varepsilon_2+(1+n)\varepsilon_m)((1+n)\varepsilon_1+(2+n)\varepsilon_m)}, \quad (1)$$

where $\varepsilon_1, \varepsilon_m$, and ε_2 are the permittivities of the RBD globule, metal (silver), and outer space (vacuum or air), respectively. The electric field excited in the metal envelope by the dipole increases when Eq. (1)

holds. The metal permittivity $\varepsilon_m(\omega) = \varepsilon_{m1}(\omega) + i\,\varepsilon_{m2}(\omega)$ has a small imaginary part $\varepsilon_{m2}(\omega)/|\varepsilon_{m1}(\omega)| << 1$. It is noteworthy that the permittivity is mostly negative in the optical and infrared spectral ranges in "good" optical metals, such as silver and gold. The resonance frequencies of the studied system ω_n are determined from Eq. (1), where $\varepsilon_m(\omega)$ is replaced with its real part $\varepsilon_{m1}(\omega)$ and the numbers n correspond to the resonance conditions for the excitation of the dipole, quadrupole, hexapole, etc., resonances. The field in the silver sphere is considerably enhanced in the case of the plasmon resonances. It may exceed the bare dipole field by orders on magnitude. When the external electric ($\mathbf{E}_e$) and magnetic ($\mathbf{H}_e$) fields are known, we can find the energy flow (Poynting vector) out of the plasmonic sphere and compare it with the flow from the bare dipole. The Raman scattering is incoherent; therefore, it is enough to average the enhancement factor G_3 over the dipoles. Thus, we find the radiation enhancement factor G_3 defined above.

In a typical Raman experiment, the excitation laser frequency ω_0 is determined by the experimental setup; therefore, the frequency $\omega = \omega_0 - \omega_s$ of the dipole is also fixed. On the other hand, the thickness d of the metal envelope may be rather easily changed in the process of the sample preparation. From Eq. 1, we can conclude that there is a resonance metal thicknesses d_{rn} for each dipole frequency ω. In our experiment, the laser wavelength was 785 nm. Using this wavelength value, we have calculated the dependences of the radiation enhancement factor $G3$ on the metal shell thickness d for wavelengths 832, 867, and 881 nm, which correspond to the most prominent Trp spectral lines with Stocks shifts of 761, 1330, and 1561 cm^{-1}, respectively (Figure 7). In this case, the radius of the metal envelope R = 130 nm is selected in such a way that its volume $4\pi R^3/3$ is equal to the typical volume of the reduced RBD aggregate (10^7 nm^3). The plot of the radiation enhancement factor is shown in Figure 8 as a function of the envelope thickness d. Indeed, one can observe the growth of enhancement factor by an order of magnitude for the metal thickness of $d \sim 10$ nm, which corresponds to the experimental values. Note that the Stokes lines with shorter wavelengths are enhanced more than those with larger wavelengths, which is also in good agreement with the experimental spectrum in Figure 7. It is supposed that the radiating dipoles are distributed in the thin layer that fills the inner surface of the sphere. The thickness of the layer is about 4 nm, which corresponds to the monolayer of the reduced RBD molecules.

As can be seen from Figure 8, the enhancement factor G_3, in general, increases with decreasing the thickness d of the metal envelope below 10 nm. On the other hand, the metal film transforms into a semicontinuous film upon decreasing its thickness. Thus, the optimal parameters of the proposed "envelope" method for SERS signal enhancement is a subject for further research.

It is natural to think that the field enhancement results in the enhancement of the dipole radiation. Usually, the dipole approximation is used to simulate the radiation of nanoparticles, because their size is

much smaller than the wavelength. However, if the dipole interacts with an optical nearfield, it experiences strong perturbations caused by field gradients. This increases the contribution of the multipoles and can lead to alteration of the selection rules. In summary, our simple spherical model qualitatively describes the enhancement of SERS from the RBD of the spike protein when it is coated with a thin silver film. Moreover, the obtained result offers the opportunity to design effective SERS sensors, where the initial SERS signal is further enhanced by the factor $G_3 >> 1$.

CONCLUSION

The main condition for the efficiency of the SERS method when applied to specific detection and diagnosis is the formation of Raman-enhancing surfaces or cavities capable of concentrating incident light within small volumes containing the analyte. The present study is the first to show that the concentration of light in metal–dielectric microcavities formed because of interaction between reduced thiol groups of the RBD of SARS-CoV-2 S glycoprotein with a silver surface allows SERS spectra to be obtained at concentrations sufficient for the detection of viral protein antigens at physiologically relevant (sub-femtogram) levels. Furthermore, an increase in the Q-factor of the microcavity via the formation of an ultranarrow nano-cleft by coating the dielectric RBD film with a nanometer-thick silver shell provides an additional tenfold enhancement of the SERS signal. Additionally, the SERS signal of the reduced RBD has been found not only to be a hundred times more intense than that of the native RBD, but also to have a completely different shape dominated by the Trp amino acid naturally buried within the protein interior and not providing any signals in either Raman or SERS spectra of native RBD. Formation of the chemical bonds between the thiol groups of reduced RBD and the surface of SERS-active substrate have been shown to activate the short-range “chemical” mechanism of Raman signals enhancement. To the best of our knowledge, this study reports the first observation of direct conversion of electromatic long-range enhancement of the protein Raman spectra to the short-range “chemical” mode of enhancement via specific reduction of protein disulfide bonds, which provokes direct interaction of not only reduced thiol, but also the aromatic Trp groups with the surface of the SERS-active substrate. Further study of the developed approach and discovered phenomenon could shed more light on the nature of this specific SERS effect and enable the development of the general approach to switching between two mechanisms of Raman signal enhancement.

Importantly, all the SERS studies dealing with the detection of SARS-CoV-2 viral particles or its protein antigens published to date either are indirect, using so-called “SERS-tags” and detecting the signals from the low-

molecular-weight Raman-reporters rather than proteins or fail to demonstrate typical protein spectra. Application of such indirect approaches make the studies of the viral antigen protein structures **and their difference in different viral variants impossible.** Our study is the first to obtain typical and characteristic Raman and SERS spectra of the RBD of S glycoprotein, the key SARS-CoV-2 viral antigen. The possibility of **direct recording of characteristic spectra of viral protein antigens** at concentrations orders of magnitude lower than those required for the detection of the whole virus in biological media makes the development of a **high-performance optical method for detecting and the pathogen variants and analyzing their conformation** a realistic task.

ACKNOWLEDGEMENT

This study was supported by the Russian Science Foundation (grant no. 21-79-30048) in the part related to the development of metal–dielectric and metal–dielectric–metal SERS-active resonators, by the Russian Foundation for Basic Research (grant no. 20-21-00080) in the parts of the development of the analytical theory and the Raman measurements, and by the Russian Foundation for Basis Research (grant no. 20-04-60440) in the part related to the SARS-Cov2 and its antigen protein preparation, bioengineering, and application to detection and diagnosis.

REFERENCES

1. C. Drosten, et al., N. Engl. J. Med. **348**, 1967 (2003).
2. T. G. Ksiazek, et al., N. Engl. J. Med. **348**, 1953 (2003).
3. A. M. Zaki, S. van Boheemen, T. M. Bestebroer, A. D. Osterhaus, and R. A. Fouchier, N. Engl. J. Med. **367**, 1814 (2012).
4. C. Huang, et al., Lancet **395**, 10223, 497 (2020).
5. Y. Zhu, et al., Nature **579**, 270 (2020).
6. P. Zhou, et al., N. Engl. J. Med. **382**, 727 (2020).
7. S. Y. Toh, M. Citartan, S. C. Gopinath, and T. H. Tang, Biosens. Bioelectron. **64**, 392 (2015).
8. C. Griffiths, S. J. Drews, and D. J. Marchant, Clin. Microbiol. Rev. **30**, 277 (2017).
9. P. Lu, Avian Dis. **47**, 361 (2003).
10. E. Spackman, et al., J. Clin. Microbiol. **40**, 3256 (2002).
11. J. Quick, et al., Nat. Protoc. **12**, 1261 (2017).
12. M. A. Tortorici and D. Veesler, Adv. Virus Res. **105**, 93 (2019).
13. I.R. Nabiev, R. G. Efremov and G. D. Chumanov, Soviet Phys. Usp. **31**, 241 (1988).
14. I. R. Nabiev, V. A. Savchenko and R. G. Efremov, J. Raman Spectrosc. **14**, 375-379 (1983).
15. I.R. Nabiev, G. D. Chumanov and R. G. Efremov, J. Raman Spectrosc. **21** 49-53 (1990).
16. A. Feofanov, V. Oleinikov, A. Tuzikov, A. Ianoul, E. Krukov, N. Bovin and I. Nabiev, Bioorg. Chem. **23**, 910-918 (1997)
17. N. L. Nechaeva, I. A. Boginskaya, A. V. Ivanov, A. K. Sarychev, A. V. Eremenko, I. A. Ryzhikov, A. N. Lagarkov, I. N. Kurochkin, *Multiscale flaked silver SERS-substrate for glycated human albumin biosensing*, Analytica Chimica Acta **1100**, 250-257 (2020).
18. I.N. Kurochkin, A.V. Eremenko, E.G. Evtushenko, N.L. Nechaeva, N.N. Durmanov, R.R. Guliev, I.A. Ryzhikov, I.A. Boginskaya, A.K. Sarychev, A.V. Ivanov, A.N. Lagarkov, *"SERS for bacteria, viruses, and protein biosensing"*, chapter 5, pp.75-94, Springer Nature Switzerland AG 75 M. Rai et al. (eds.), Macro, Micro, and Nano-Biosensors, (2021).
19. T. Deckert-Gaudig, A. Taguchi, S. Kawata and V. Deckert, *Tip-enhanced Raman spectroscopy – from early developments to recent advances"*, Chem. Soc. Rev., **46**, 4077 (2017).
20. A. Taguchi, J. Yu, P. Verma and S. Kawata, *Optical antennas with multiple plasmonic nanoparticles for tip-enhanced Raman microscopy*, Nanoscale, **41**, DOI: 10.1039/C5NR05022G2015 (2017).

21. L. Huang, L. Din, J. Zhou, S. Chen, F. Chen, C. Zhao, J. Xu, W. Hu, J. Ji, H. Xu, G.L. Liu, *One-step rapid quantification of SARS-CoV-2 virus particles via low-cost nanoplasmonic sensors in generic microplate reader and point-of-care device*, Biosensors and Bioelectronics, **171**, 112685 (2020),
22. T. Stanborough, F.M. Given, B. Koch, C.R. Sheen, A.B. Stowers-Hull, M.R. Waterland, and D.L. Crittenden, *Optical detection of CoV-SARS‑2 viral proteins to sub-picomolar concentrations*, ACS Omega, **6**, 6404−6413 (2021).
23. D. Zhang, X. Zhang, R. Ma, S. Deng, X. Wang, X. Wang, X. Zhang, X. Huang , Y. Liu, G. Li, J. Qu, Y. Zhu, J. Li, *Ultra-fast and onsite interrogation of Severe Acute Respiratory Syndrome Coronavirus 2 (SARS-CoV-2) in waters via surface enhanced Raman scattering (SERS),* Water Research, **200** 117243 (2021)
24. J.E. Sanchez, S.A. Jaramillo, E. Settles, J. J.V. Salazar, A. Lehr, J. Gonzalez, C.R. Aranda, H.R. Navarro-Contreras, M.O. Raniere, M. Harvey, D.M. Wagner, A. Koppisch, R. Kellar, P. Keimb and M.J. Yacaman, *Detection of SARS-CoV-2 and its S and N proteins using surface enhanced Raman spectroscopy*, RSC Adv., **11**, 25788 (2021).
25. C. Carlomagno, D. Bertazioli, A. Gualerzi, S. Picciolini, P.I. Banfi, A. Lax, E. Messina, J. Navarro, L. Bianchi, A. Caronni, F. Marenco, S. Monteleone, C. Arienti & M. Bedoni, *COVID‑19 salivary Raman fingerprint: innovative approach for the detection of current and past SARS‑CoV‑2 infections*, Scientific Reports **11**:4943 (2021).
26. E. Zavyalova, et al., *SERS-based aptasensor for rapid quantitative detection of SARS-CoV-2*, Nanomaterials, **11**, 1394 (2021).
27. M. Zhang, X. Li, J. Pan, Y. Zhang, L. Zhang, C. Wang, X. Yan, X. Liu, G. Lu, *Ultrasensitive detection of SARS-CoV-2 spike protein in untreated saliva using SERS-based biosensor*. Biosensors & Bioelectronics **190**, 113421 (2021).
28. J. Lan, J. Ge, J. Yu, S. Shan, H. Zhou, S. Fan, Q. Zhang, X. Shi, Q. Wang, L. Zhang, and X. Wang, Nature **581**, 215 (2020)
29. J. De Gelder, K. De Gussem, P. Vandenabeele and L. Moens, *Reference database of Raman spectra of biological molecules*. J. Raman Spectrosc.; **38**: 1133–1147 (2007).
30. A.K. Sarychev, A. Ivanov, A.N. Lagarkov, G. Barbillon, I. Ryzhikov, I. Bykov, K. Afanasev, N. Bakholdin, M. Mikhailov, A. Smyk, A. Shurygin, A. Shalygin, *Holographic metasurfaces for SERS sensors*, in press.
31. A.K. Sarychev, A. Ivanov, A. Lagarkov and G. Barbillon, Materials **12**, 103 (2019)

32. S. Gresillon, L. Aigouy, A.C. Boccara, J.C. Rivoal, X. Quelin, C. Desmarest, P. Gadenne, V.A. Shubin, A.K. Sarychev, V.M. Shalaev, *Experimental observation of localized optical excitations in random metal-dielectric films*, Phys. Rev. Lett. **82**, 4520 (1999).
33. Z.-Q. Tian, B. Ren and D.-Y. Wu, *Surface-enhanced Raman scattering: from noble to transition metals and from rough surfaces to ordered nanostructures*. J. Phys. Chem. B, **106**, 9464-9483 (2008).
34. S.-Y. Ding, J. Yi, J.-F. Li, B. R., D.-Y. Wu, R. Panneerselvam and Z.-Q. Tian, *Nanostructure-based plasmon enhanced Raman spectroscopy for surface analysis of materials*, Nature Rev., **1**, 1-16 (2016).

FIGURE CAPTIONS

Figure 1. The three-dimensional structure of the receptor-binding domain (RBD) of the SARS-CoV-2 S glycoprotein. RBD is shown in cyan, and the receptor-binding motif (RBM) of this protein, which interacts with the cell receptor, is shown in red. The SARS-CoV-2 RBD disulfide bonds are shown in yellow and marked with arrows. The figure is adapted from Ref. [28].

Figure 2. AFM images of the metal surface of surface-enhanced Raman scattering (SERS)-active substrates without protein samples applied. The left panel shows a 40×40 μm area; the right panel shows the image obtained in the area marked with a blue square in the left panel (7×7 μm); the bottom panel shows the cross section along the green line in the right panel.

Figure 3. Left: A sketch illustrating the method for fabricating a metal-dielectric microcavity consisting of a dielectric protein globule of receptor-binding domain (RBD) and the metal surface of the surface-enhanced Raman scattering (SERS)-active substrate. The reduction of all four disulfide bonds of the RBD protein results in the formation of an additional eight free sulfhydryl groups capable of forming strong chemical bonds with silver atoms. The unfolding of the protein globule as a result of disulfide bond reduction leads to spatial approximation between the tryptophan (Trp) residues and the surface of the SERS-active substrate and the dominance of Trp in the SERS spectrum (Figures 6, 7).

Right: A sketch of the structure of the native RBD of the SARS-CoV-2 S glycoprotein applied onto the silver surface of the surface-enhanced Raman scattering (SERS)-active substrate. The distances between the surface of the SERS-active substrate and two Trp residues of the RBD amino acid sequence located deep in the protein globule are indicated. The data were calculated from the atomic coordinates of the three-dimensional structure of the RBD protein reported in [20].

Figure 4. AFM images of the silver surface of surface-enhanced Raman scattering (SERS)-active substrates with a sample of the receptor-binding domain (RBD) of the SARS-CoV-2 S glycoprotein with reduced disulfide bonds applied onto it. The left panel shows a 40×40 μm area; the right panel shows the image obtained in the area marked with a blue square in the left panel (9×9 μm); the bottom panel shows the cross section along the green line in the right panel.

Figure 5. Finding and mapping a sample of the receptor-binding domain (RBD) protein with reduced disulfide bonds (upper panels) and an additional silver layer applied onto the protein dielectric film (lower panels). Protein samples were applied onto the metal surface of the surface-enhanced Raman scattering (SERS)-active substrate for spectral studies. The left panels show images in the wide-field upright optical microscopy mode. The right panels show mapping in the confocal mode based on the Raman scattering characteristic band (the tryptophan line at about 755 cm^{-1}) for subsequent recording of the SERS spectrum at the point indicated by the green cross.

Figure 6. Raman scattering and surface-enhanced Raman scattering (SERS) spectra of the receptor-binding domain (RBD) of the SARS-CoV-2 S glycoprotein.

(1) An unenhanced Raman spectrum obtained from native SARS-Cov-2 RBD from a dried drop on a glass slide. The Raman signal is collected from a focus spot with a volume estimated at 10^9 nm^3, which contains about **1.3 pg** of RBD. The scaling factor for the integrated intensity of the spectrum is 126.

(2) A SERS spectrum obtained from 3 fg of the sample of native SARS-Cov-2 RBD in a single aggregate on the silver surface of the SERS-active substrate. The scaling factor for the integrated intensity is 216.

(3) A SERS spectrum obtained from 3 fg of the sample of SARS-Cov-2 RBD with reactive thiol groups (reduced disulfide bonds) on the silver surface of the SERS-active substrate. The scaling factor for the integrated intensity is 1.

(4) A Raman – SERS difference spectrum demonstrating the SERS effect expressed in variation of the relative intensities of some Raman bands on the SERS-active substrate.

Figure 7. Changes in the degree of enhancement of the Raman scattering spectrum of a sample of the receptor-binding domain (RBD) of the SARS-CoV-2 S glycoprotein with reactive thiol groups upon application of a thin silver film onto the protein sample bound with the surface-enhanced Raman scattering (SERS)-active substrate.

(1) The SERS spectrum of RBD upon additional application of a thin silver film onto the protein sample bound to the surface of the SERS-active substrate. The spectrum is not normalized.

(2) The SERS spectrum of RBD without additional application of a thin silver film onto the protein sample bound to the surface of SERS-active substrate. The normalization factor for the tryptophan residue band at about 755 cm^{-1} is 9.0.

Figure 8. Enhancement of the Raman signal from the layer of molecular dipoles as function of silver thickness *d*. The molecular dipoles are distributed over internal surface of the silver sphere of radius R =

130 nm; the thickness of the molecular monolayer is 4 nm. Dipoles radiate with wavelengths λ = 834, 867, and 881 nm (brown, red, and orange curves); the enhanced Raman signal from the plasmon resonator is normalized to Raman signal generated the bare molecular monolayer.

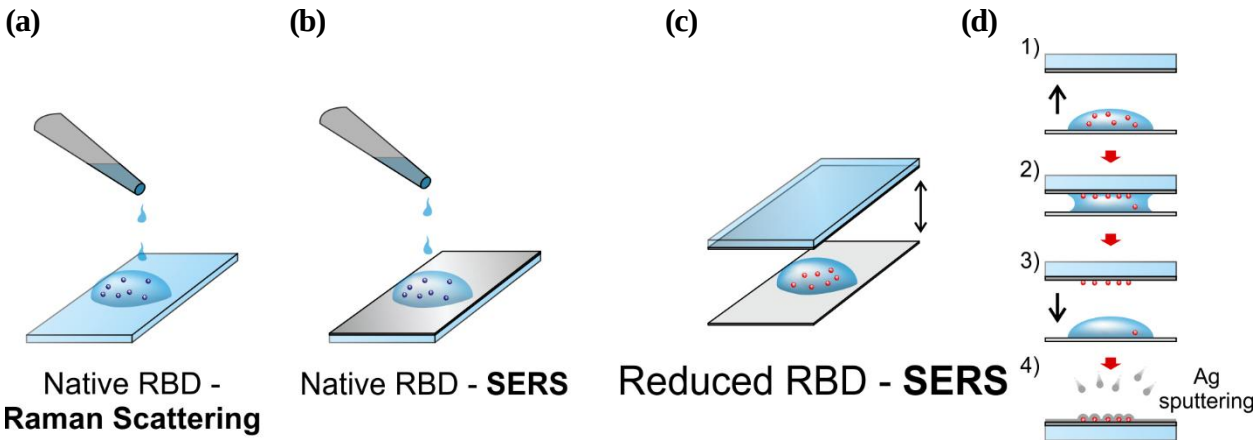

Scheme 1.

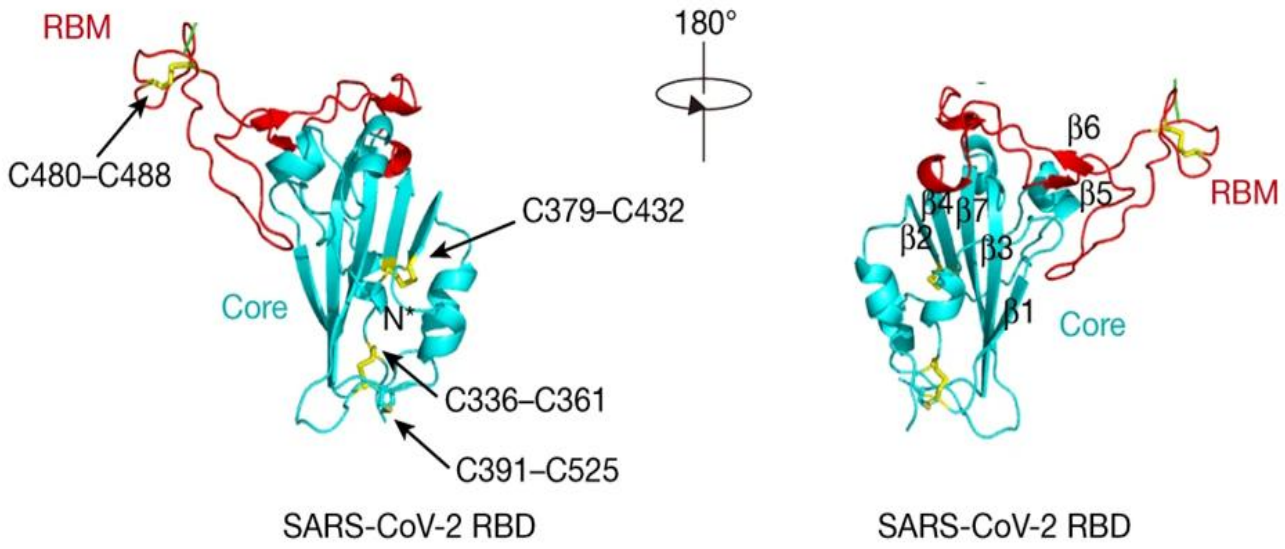
RBM
C480–C488
180°
C379–C432
Core
N*
C336–C361
C391–C525
SARS-CoV-2 RBD
β6
β5
RBM
β4
β7
β2
β3
β1
Core
SARS-CoV-2 RBD

Figure 1

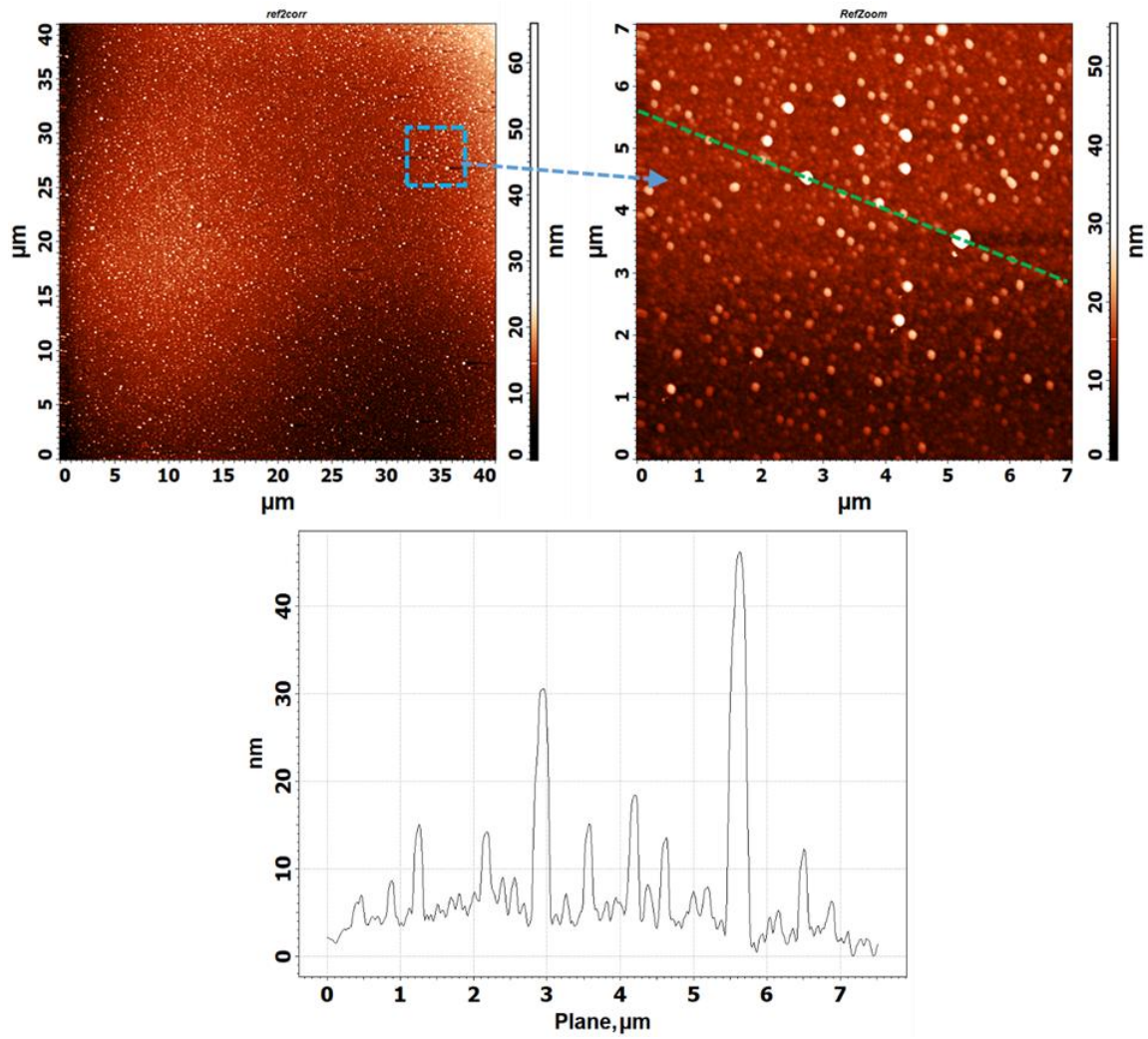

Figure 2

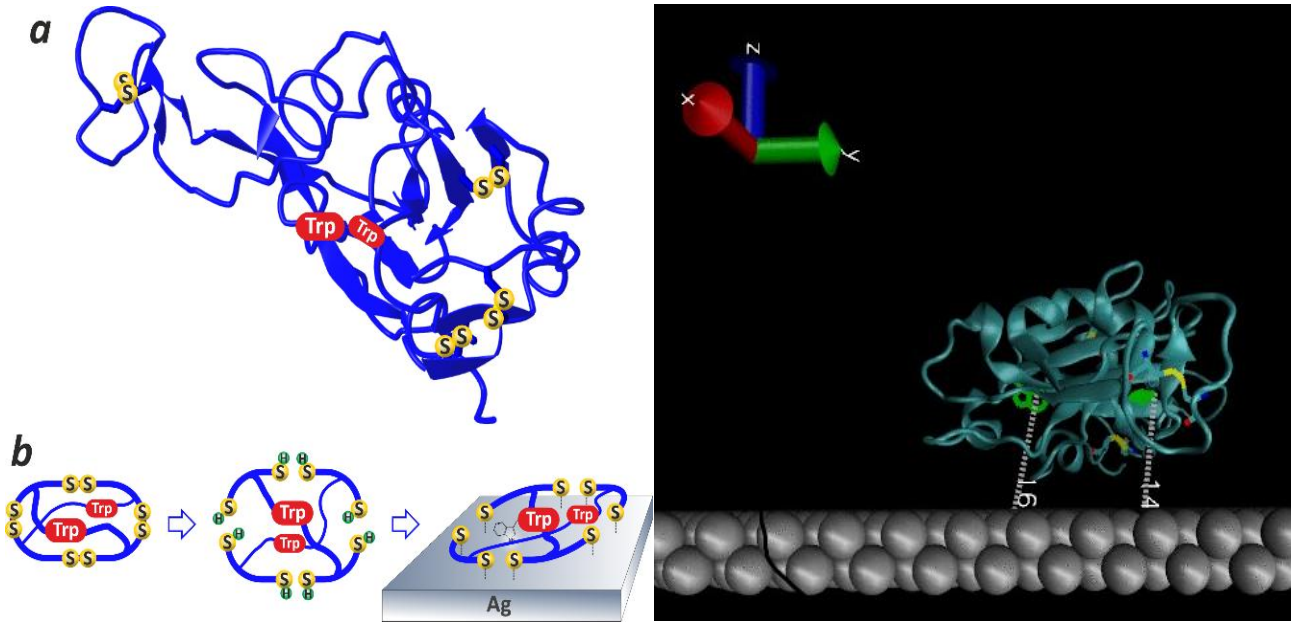

Figure 3

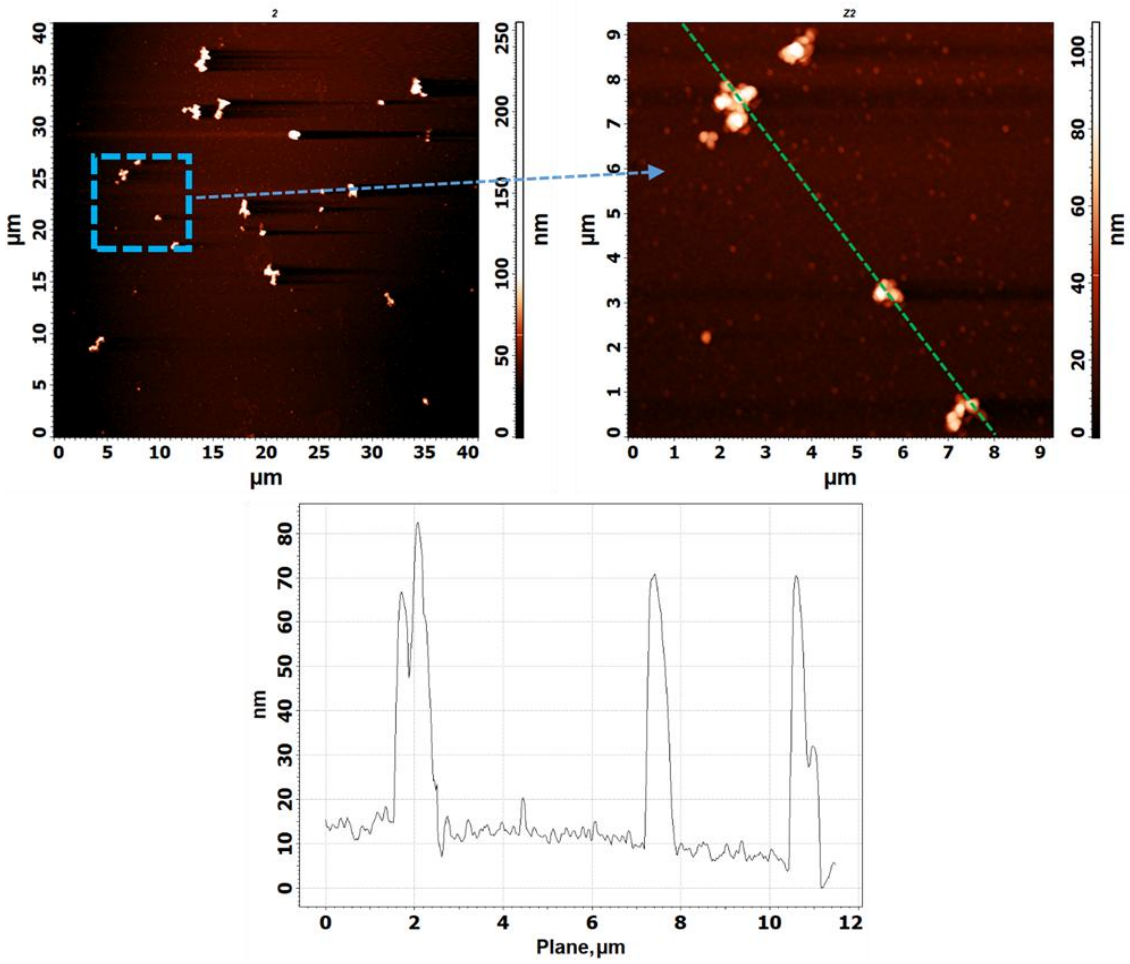

Figure 4

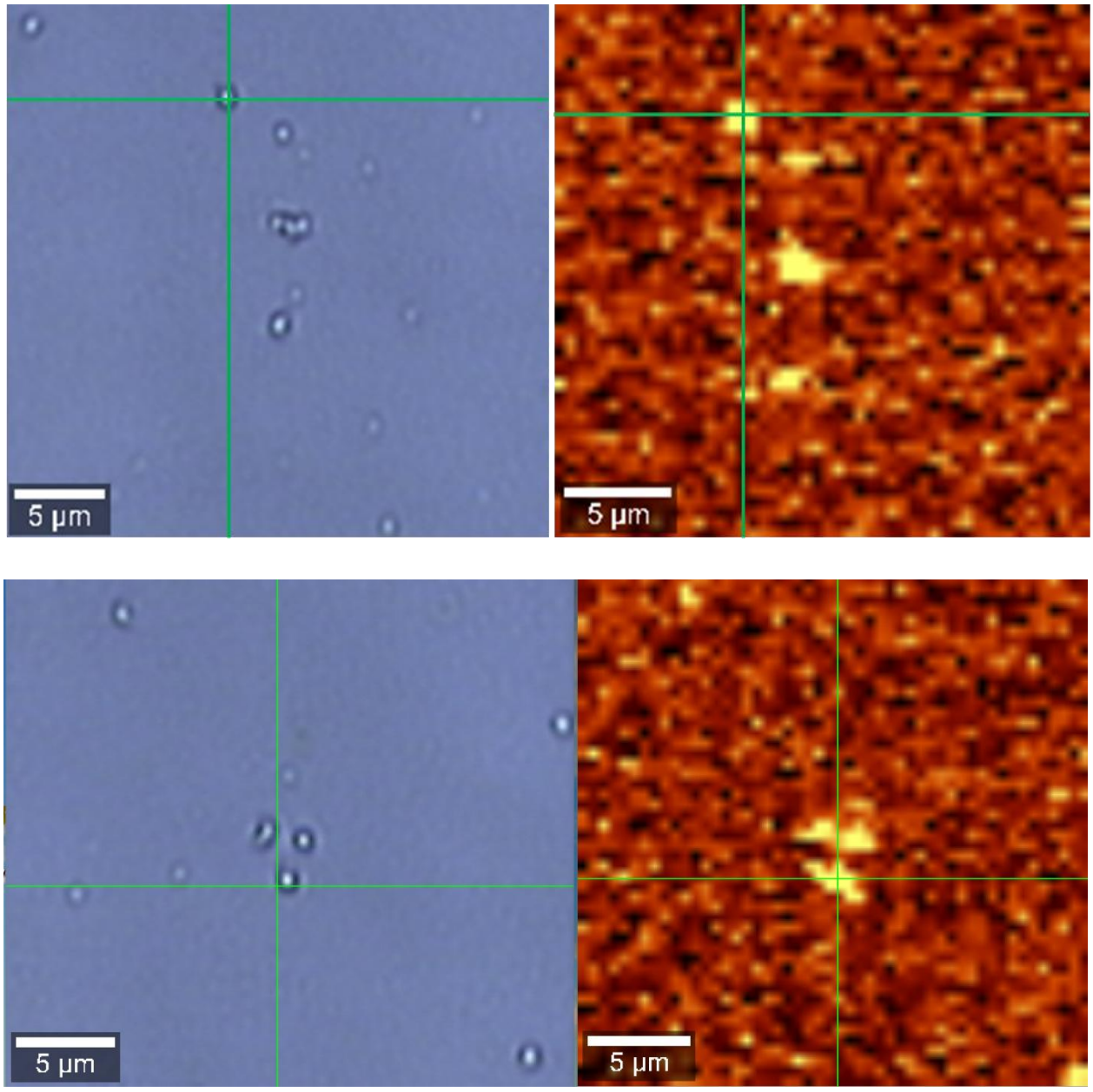

Figure 5

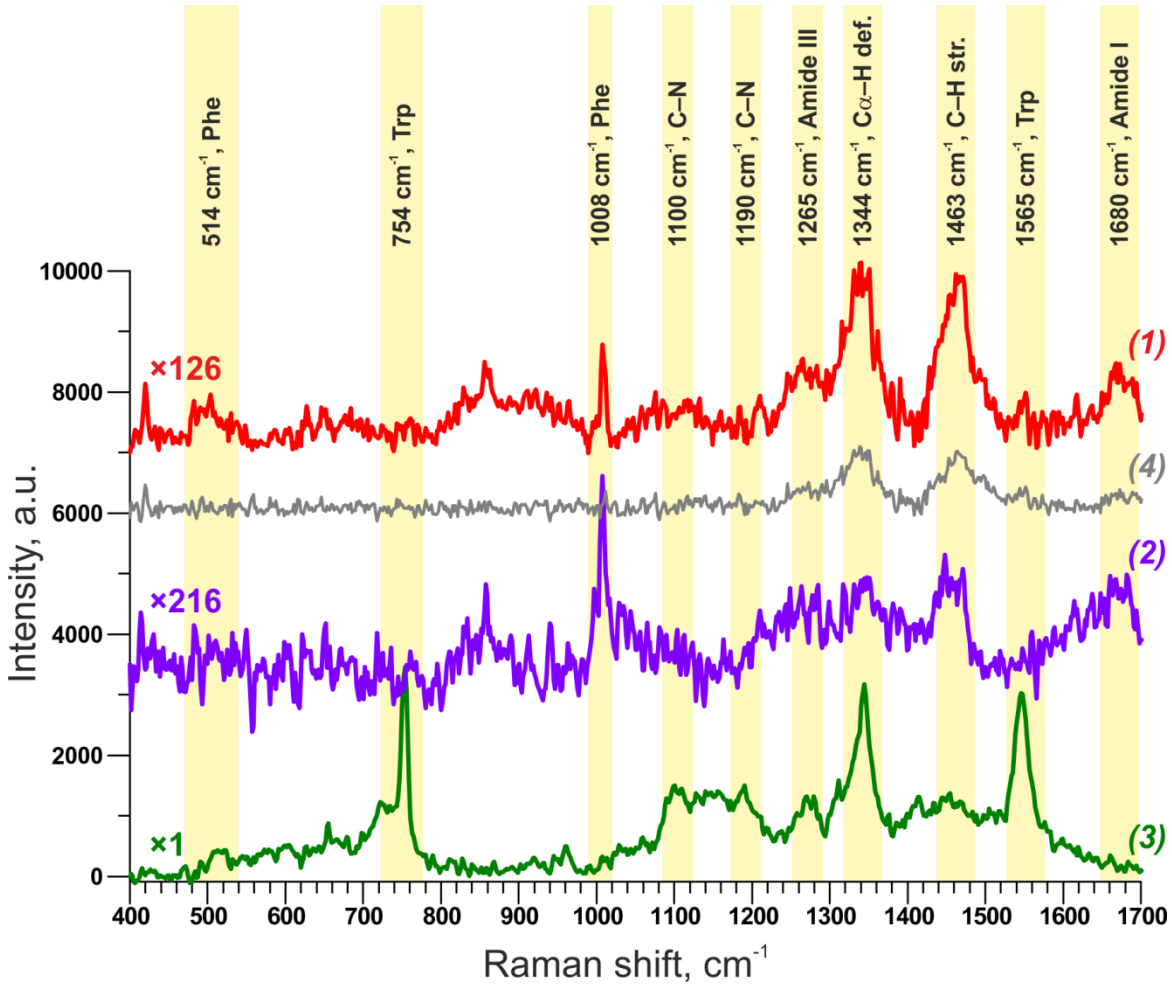
514 cm-1, Phe
754 cm-1, Trp
1008 cm-1, Phe
1100 cm-1, C–N
1190 cm-1, C–N
1265 cm-1, Amide III
1344 cm-1, Cα–H def.
1463 cm-1, C–H str.
1565 cm-1, Trp
1680 cm-1, Amide I
×126
×216
×1
(1)
(2)
(3)
(4)
Intensity, a.u.
Raman shift, cm-1

Figure 6

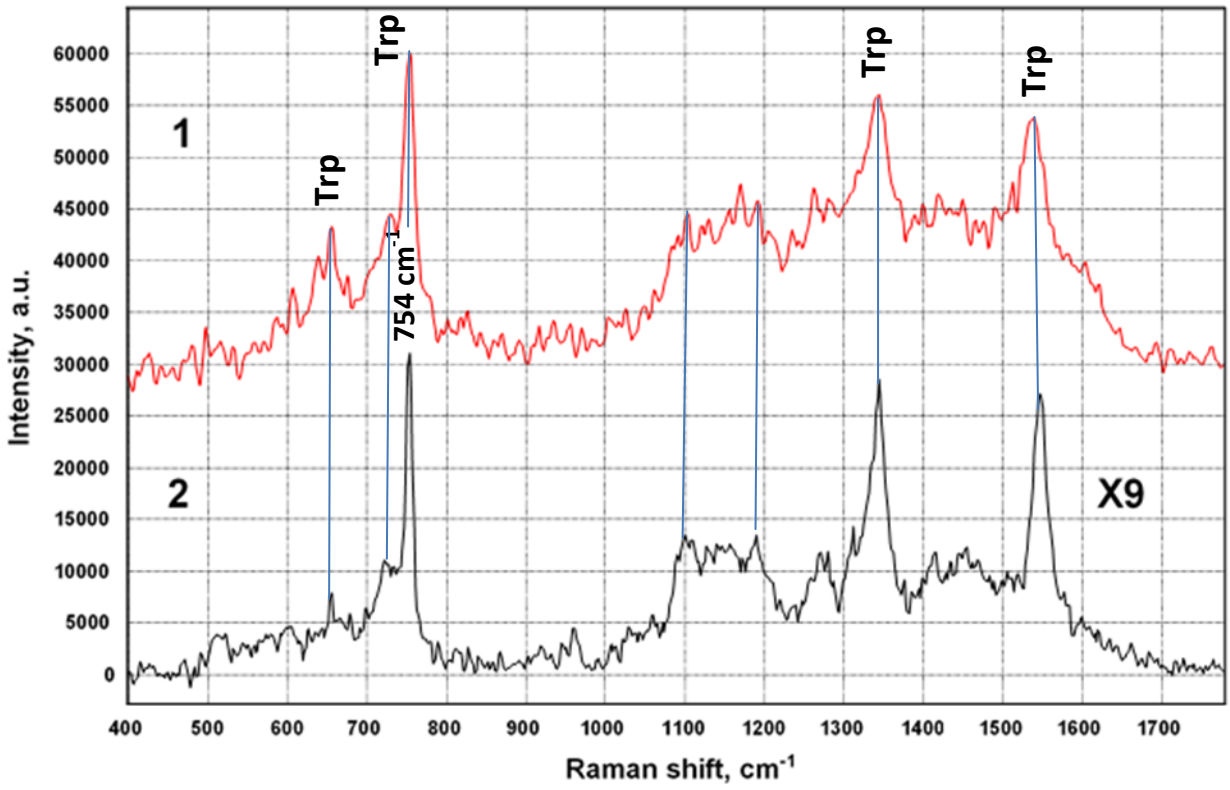
Trp
Trp
Trp
Trp
754 cm-1
1
2
X9
Intensity, a.u.
Raman shift, cm-1
60000
55000
50000
45000
40000
35000
30000
25000
20000
15000
10000
5000
0
400
500
600
700
800
900
1000
1100
1200
1300
1400
1500
1600
1700

Figure 7

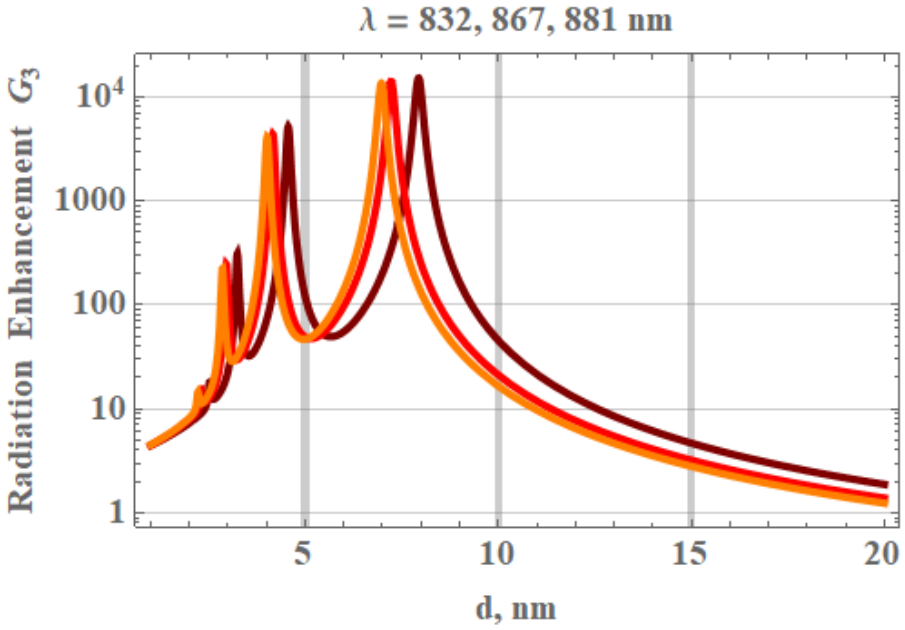
λ = 832, 867, 881 nm
Radiation Enhancement G_3
10^4
1000
100
10
1
5
10
15
20
d, nm

Figure 8

Suppl. Table S1. Spike-protein's RBD-domain: sequence and properties.

```
319                 329                 339                 349
RVQPTESIVR FPNITNLC1PF GEVFNATRFA SVYAWNRKRI

359                 369                 379                 389
SN C1VADYSVL YNSASFSTFK C2YGVSPTKLN DLC3FTNVYAD

399                 409                 419                 429
SFVIRGDEVR QIAPGQTGKI ADYNYKLPDD FTG C2VIAWNS

439                 449                 459                 469
NNLDSKVGGN YNYLYRLFRK SNLKPFERDI STEIYQAGST

479                 489                 499                 509
PC4NGVEGFNC4 YFPLQSYGFQ PTNGVGYQPY RVVVLSFELL

519                 529                 539
HAPATVC3GPK KSTNLVKNKC VNF
```

Molecular weight: 25 098.40 Da

Theoretical pI: 8.91

Amino-acids composition (223 amino-acids):

Ala (A)	12	5.4%
Arg (R)	11	4.9%
Asn (N)	21	9.4%
Asp (D)	9	4.0%
Cys (C)	**9**	**4.0%**
Gln (Q)	7	3.1%
Glu (E)	7	3.1%
Gly (G)	15	6.7%
His (H)	1	0.4%
Ile (I)	9	4.0%
Leu (L)	14	6.3%
Lys (K)	12	5.4%
Met (M)	0	0.0%
Phe (F)	**16**	**7.2%**
Pro (P)	13	5.8%
Ser (S)	17	7.6%
Thr (T)	13	5.8%
Trp (W)	**2**	**0.9%**
Tyr (Y)	**15**	**6.7%**
Val (V)	20	9.0%